OBSERVED BEHAVIOR OF SEISMICALLY ISOLATED BUILDINGS

By Jonathan P. Stewart,[1] Joel P. Conte,[2] and Ian D. Aiken,[3] Members, ASCE

ABSTRACT: Strong motion recordings from four seismically isolated buildings are used in time-invariant and time-variant modal identification analyses. The buildings are identified as equivalent, time-varying, linear dynamic systems characterized by their time-varying modal parameters (including fundamental-mode natural frequencies, damping ratios, and mode shapes). The identification analyses for each site are repeated using multiple earthquake recordings. In the case of one building, the inferred isolator stiffness and damping during several earthquakes is compared with experimental results. Spectral displacements of the ground motion at the effective fundamental period of the seismically isolated building are found to correlate well with two measures of isolator behavior—the maximum reduction in fundamental mode frequency during strong shaking, and the fraction of the peak total building deformation occurring within the isolators. While the recorded ground motions have much smaller amplitudes than the design basis motions, extrapolation of the observed trends in frequency reduction and relative isolator deflection to larger levels of shaking indicates performance estimates consistent with those assumed in design (which were based on laboratory testing of the isolators).

INTRODUCTION

Seismic isolation involves introducing to a structure a plane of lateral flexibility that is intended to significantly lengthen the structure's fundamental period, shifting it away from the destructive frequency range of typical ground motions. In buildings, the lateral flexibility is often achieved through the use of elastomeric bearings, usually near the base of the structure. Several key assumptions influence the design of seismically isolated structures:

1. A significant increase in both fundamental-mode period and damping accompanies the addition of isolators to the structure's lateral force resisting system (fundamental period increases of 1.5–3 times are typical, while damping increases from a few percent to greater than 10% are common).
2. Lateral deformations are concentrated in the isolators, and in many cases the remainder of the structure is assumed to behave relatively stiffly (perhaps even rigidly), thus providing no significant dynamic amplification over the height of the building.
3. The dependence of isolator response on its deformation history is neglected, i.e., the fully developed isolator flexibility and damping is assumed to act during the entire duration of strong ground shaking.

Previous research investigating the performance of seismically isolated buildings has focused on (1) the Foothill Communities Law and Justice Center (FCLJC) Building response to the 1985 Redlands and 1990 Upland earthquakes (Papageorgiou and Lin 1989; Kelly et al. 1991; Maison and Ventura 1992), (2) the Los Angeles 2-Story Fire Command and Control Building response to the 1994 Northridge earthquake (Nagarajaiah and Xiahong 1995), (3) the Los Angeles 7-story USC Hospital response to the 1994 Northridge earthquake (Nagarajaiah and Xiahong 1995), and (4) the response of a residential building in Los Angeles supported on helical steel springs and viscoelastic-fluid-filled dampers to the Northridge earthquake (Makris and Deoskar 1996). All of these studies have used time-invariant system identification procedures to infer response parameters, which in turn are used to validate existing linear and nonlinear analysis techniques and design criteria used for seismically isolated structures.

The intent of this paper is to document the seismic behavior of four seismically isolated buildings from their recorded response for earthquakes producing various amplitudes and durations of shaking. Through appropriate recursive system identification procedures, these buildings are identified as equivalent, time-varying, linear dynamic systems, characterized by their time-varying modal parameters (fundamental-mode natural periods, damping ratios, and mode shapes). The results are used to verify key assumptions made in the design of isolated buildings and to shed new light on the actual earthquake response mechanisms of isolated buildings. Also reviewed is the influence of soil-structure interaction (SSI) on the observed response. In contrast with previous works, this paper (1) achieves new insights into isolation system behavior by examining temporal variations in system properties, using recursive system identification analysis; (2) considers the responses of multiple buildings to multiple earthquakes, using consistent procedures; and (3) formally evaluates soil-structure interaction effects that have been neglected a priori in previous studies.

SITES CONSIDERED

Four seismically isolated buildings are considered in this paper, each of which has recorded shaking from multiple earthquakes. Structural, geotechnical, and ground motion information for these buildings are discussed in detail in Stewart and Stewart (1997). Key attributes are summarized here and in Table 1.

Los Angles Two-Story Fire Command and Control Building (LA2FCCB)

The building is two stories tall with no basement and has a rectangular shape in plan (26 by 57 m). The lateral load-resisting system consists of perimeter steel inverted chevron braced frames and 32 high damping rubber bearings to provide seismic isolation below the 1st floor. The building is founded on spread footings resting on weathered siltstone bedrock. Accelerometers are present at the foundation level (below the isolators), 1st floor (above the isolators), 2nd floor and roof.

Los Angeles Seven-Story USC Hospital (LA7USC)

The building is seven stories tall with a partial basement and has an irregular shape, with maximum plan dimensions of

[1]Asst. Prof., Civ. and Envir. Engrg. Dept., Univ. of California, Los Angeles, CA 90095.
[2]Assoc. Prof., Civ. and Envir. Engrg. Dept., University of California, Los Angeles, CA.
[3]Prin., Seismic Isolation Engineering, Oakland, CA 94611.

Note. Associate Editor: Takeru Igusa. Discussion open until February 1, 2000. To extend the closing date one month, a written request must be filed with the ASCE Manager of Journals. The manuscript for this paper was submitted for review and possible publication on February 9, 1999. This paper is part of the ***Journal of Structural Engineering***, Vol. 125, No. 9, September, 1999. ©ASCE, ISSN 0733-9445/99/0009-0955–0964/$8.00 + $.50 per page. Paper No. 20227.

TABLE 1. Transverse Fixed-Base Structural Parameters and Earthquake Ground Motion Indexes for Subject Sites

Site (1)	Earthquake (2)	Building height (m) (3)	Top of isolator (m) (4)	Free-field PGA (g) (5)	Whole Building (Including Isolators)				Above Isolators			
					Delay, d (time steps) (6)	Number of modes, j (7)	CEM period (sec) (8)	CEM damping (%) (9)	Delay, d (time steps) (10)	Number of modes, j (11)	CEM period (sec) (12)	CEM damping (%) (13)
1. LA 2-story	Sierra Madre*	10	0.3	0.113	1	6	0.79	10.6	0	6	0.43	10.2
	Landers*	—	—	0.048	0	6	0.98	15.5	0	6	0.48	15.3
	Northridge*	—	—	0.320	4	6	0.90	38.4	—	—	—	—
2. LA 7-story	Landers*	36	0.3	0.043	4	7	1.18	12.1	5	7	0.90	4.2
	Northridge	—	—	0.214	5	8	1.27	29.3	4	7	0.87	10.0
3. FCLJC	Redlands	24	1.7	0.040	2	6	0.59	3.7	0	6	0.50	6.0
	Whittier	—	—	0.046	2	6	0.63	5.0	2	6	0.53	4.6
	Upland	—	—	0.240	3	6	0.77	7.8	4	6	0.68	6.3
	Landers	—	—	0.112	3	6	0.85	12.5	0	6	0.62	4.0
	Northridge	—	—	0.072	3	6	0.75	6.9	1	6	0.62	5.8
4. SB 8-story	Landers	40	8.5	0.044	5	6	1.25	13.2	4	6	0.93	7.3
	Northridge	—	—	0.061	3	6	1.18	7.1	3	6	0.94	3.8

Note: * = pseudo flexible-base parameters, rocking effect not removed.

77 × 92 m. The lateral load-resisting system consists of diagonally braced perimeter steel frames and lead-rubber and natural rubber isolators below the lower level. The foundation consists of spread footings with grade beams resting on shallow soils overlying weathered siltstone and shale bedrock. Accelerometers are present at the foundation level (below the isolators), lower level (above the isolators), 4th and 6th stories, and roof.

Foothill Communities Law and Justice Center (FCLJC) in Rancho Cucamonga

The building is four stories tall above ground level, with a single level basement. The structure has a rectangular shape, with plan dimensions of 34 × 126 m. The lateral load-resisting system consists of braced steel frames in the upper four stories and concrete shear walls in the basement. The isolation system consists of 98 high-damping rubber bearings below the basement level. All of the bearings are 76 cm in diameter and about 46 cm in height, with a total rubber height of about 30.5 cm. The foundation consists of spread footings resting on 1–3 m of aeolian sand overlying deep alluvial fan deposits. Accelerometers are present at the foundation level (below the isolators), basement (above the isolators), 2nd floor, and roof.

Seal Beach 8-Story Building (SB8)

The building is eight stories tall with a single-level stepped basement and is rectangular in plan; the dimensions are 42 × 75 m. Originally designed in 1967, the structure was retrofitted in 1990 by installing isolators in the columns between the 1st and 2nd floors, and by stiffening the exterior concrete frames. The foundation consists of concrete piers, typically 1 m in diameter and 15 m long, founded in about 8 m of silty clay overlying dense sands and clays. Accelerometers are present at the basement and roof levels, as well as the 1st, 2nd, and 6th floors.

SYSTEM IDENTIFICATION RESULTS

The seismic behavior of the four seismically isolated buildings is examined through system identification analysis. After a brief review of the system identification procedures used herein, detailed results are given for the FCLJC and general results are given for all four buildings.

System Identification Analysis Procedures

Parametric system identification procedures were used to evaluate the fundamental-mode vibration parameters and mode shapes for the four subject buildings. These procedures estimate a Laplace domain transfer function relating a single input motion to a single output. The amplitude of the complex-valued transfer function forms a surface in the Laplace domain, with peaks located at poles whose locations can be mapped to modal vibration parameters (frequency and damping) using procedures in Safak (1991) and Stewart and Fenves (1998). In addition, the intersection of the transfer function surface with the complex plane (which is the frequency axis) provides a frequency-domain transmissibility function relating the input and output motions. Peaks in the transmissibility function occur at modal frequencies, and the amplitude of the peaks is related to the amplification of the output relative to the input at the corresponding frequency. Fundamental-mode shapes were estimated from a suite of relative transmissibility function amplitudes (at the first-mode frequency) identified using response records from sensors located at various heights throughout the structure, while keeping the same input motion.

Transfer functions can be estimated by minimizing cumulative error for the entire time history (cumulative error method, CEM) (Safak 1991), or by recursively minimizing error for each time step using a time window (modulated with an exponentially decaying function) immediately preceding that time step (recursive prediction error method, RPEM) (Safak 1989a,b). For either CEM or RPEM analyses, two parameters are selected by the analyst, the time delay between the input and output (d) and the number of modes included in the analysis (j). For a given structure, these parameters are identical for CEM or RPEM analyses, and are listed in Table 1 for the subject sites. The modal parameters obtained through CEM identification represent average, effective, linear dynamic characteristics of the actual nonlinear structure over the entire response history. The recursive analyses identify time-varying modal parameters of an equivalent, time-variant, linear dynamic model of the actual nonlinear structural system and are useful for evaluating the intra-event variability of the nonlinear hysteretic isolator response. The parameter governing the width of the exponentially decaying time window was selected as $\lambda = 0.99$ (the results for the subject sites were fairly insensitive to this parameter). Safak (1989b) has verified the results of RPEM analyses against simpler and more approximate methods of system identification, such as Fourier analyses.

In general, the input and output motions used in the identifications can include free-field, foundation-level, and roof translations, as well as foundation-level rocking. Stewart and Fenves (1998) defined the various sources of stiffness in the

TABLE 2. Sources of System Stiffness for Different Input-Output Pairs

Input (1)	Output (2)	Sources of system stiffness[a] (3)	Base fixity (4)
Free-field translation	Roof translation	k, k_θ, k_U	Flexible-base
Base translation	Roof translation	k, k_θ	Pseudo-flexible-base
Base translation + contribution of base rocking to roof translation	Roof translation	k	Fixed-base

[a] k = structural stiffness; k_U = soil-foundation stiffness in translation; k_θ = soil-foundation stiffness in rocking.

soil-foundation-building system captured by system identification results for various combinations of input/output data pairs. These results are summarized in Table 2. In the context of this paper, ''fixed-base'' refers to a system that includes only structural flexibility, that is soil-foundation flexibility in translation and rocking is removed. Note the distinction from the traditional isolation literature, in which ''fixed-base'' refers to the properties of a superstructure above the level of the isolators.

The strong-motion instrument arrays at the subject sites enable direct identification of fixed- and flexible-base parameters for the LA7USC, FCLJC, and SB8 buildings. LA2FCCB lacks base-rocking instrumentation, so fixed-based parameters cannot be directly evaluated but nevertheless can be estimated from pseudo-flexible-base and flexible-base parameters using procedures developed by Stewart and Fenves (1998). Reported in Table 1 are fixed-base modal parameters for each of the subject buildings and earthquakes, with the exception of LA2FCCB and the Landers recording at LA7USC, for which pseudo-flexible-base parameters are reported.

Results for FCLJC

For each of the five earthquakes recorded at FCLJC, the following suites of system identification analyses were performed using transverse (North-South) response motions:

1. RPEM analysis of pseudo-flexible-base response to obtain time-varying, first-mode vibration parameters.
2. CEM and RPEM analyses of pseudo-flexible-base response to obtain first-mode shapes.

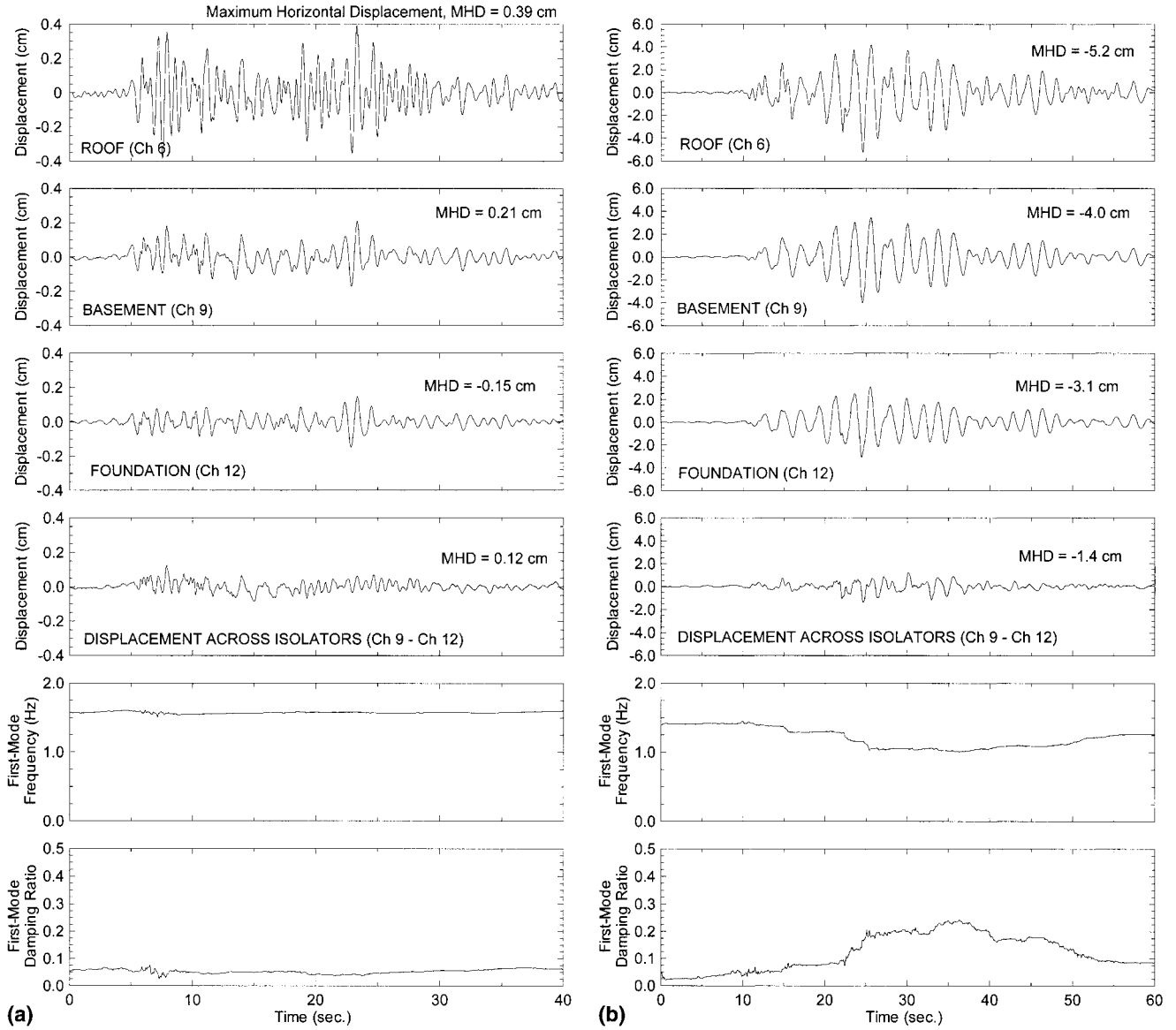

FIG. 1. Displacement Time Histories and Time Variation of First-Mode Parameters: (a) FCLJC, 1987 Whittier Earthquake (Transverse, NS Direction); (b) FCLJC, 1992 Landers Earthquake (Transverse, NS Direction)

3. CEM analysis of fixed-, flexible-, and pseudo-flexible-base response to evaluate the significance of inertial soil-structure interaction effects.

Pseudo-flexible-base response is considered in 1 and 2 in order to maintain consistency in the RPEM and mode shape analysis for all sites (since fixed-base response cannot be directly evaluated at LA2FCCB). However, as shown below, differences between pseudo-flexible- and fixed-base response are negligible for all four buildings. For the sake of brevity, the FCLJC responses to the 1987 Whittier and 1992 Landers earthquakes are discussed in detail here to illustrate the variability in isolated building response for weak and moderate intensity ground shaking. Results for other earthquakes are reviewed briefly and are consistent with the trends from the two selected events.

Displacements recorded at the roof, basement level (above isolators), and foundation level (below isolators) during the two earthquakes are shown in the first to third frames of Figs. 1(a and b). The relative displacement across the isolators is plotted in frame four. The Whittier earthquake produced fairly weak motions at the site that were of short duration, whereas the Landers earthquake produced motions of moderate amplitude but with much lower frequency content and longer duration. The bottom two frames of the figures show the time variation of the first mode frequency and damping ratio. In the case of the Whittier earthquake [Fig. 1(a)], the structural response (including the isolators) is seen to be time invariant, indicating that no significant nonlinearity or ''softening'' developed in the isolators during the relatively weak shaking. The identified frequency of about 1.59 Hz and 5% damping are reasonably consistent with modal vibration parameters, identified from ambient vibration tests by Pardoen and Hart (1985), of 1.75 Hz and 2.3% damping. These ambient vibration studies were performed on the steel frame of the building during construction; hence, the identified modal parameters represent properties of the structural skeleton under very small isolator shear strains. The larger strains from the Whittier earthquake, and the added mass in the completed building, could readily account for the differences in the fundamental-mode parameters. In contrast to the time invariant Whittier response, the relatively strong shaking from the Landers earthquake produced significant reductions in effective fundamental frequency, and increases in effective damping ratio, during early portions of the time history when the amplitude of shaking was increasing (t < 25 s). These data suggest that the effective linear vibration properties of the isolated structure are strongly dependent on intensity of shaking.

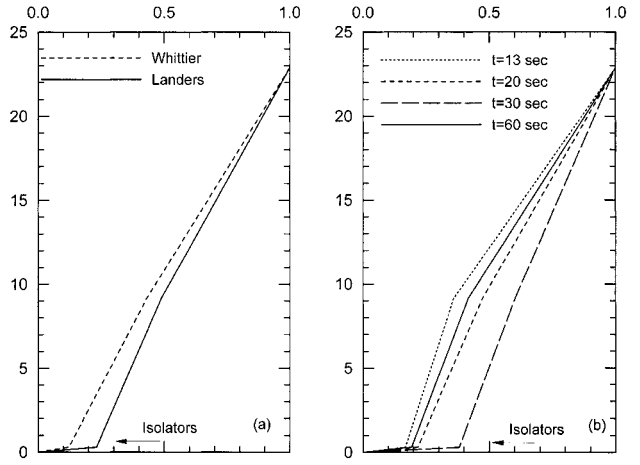

FIG. 2. Mode Shapes for FCLJC: (a) Comparison of CEM Results for Whittier and Landers Earthquakes; (b) RPEM Results for Landers

TABLE 3. First-Mode Parameters for Various Base Fixity Conditions, with Calculated Period Lengthening and Foundation Damping, FCLJC

Earthquake (1)	Flexible-Base $\tilde{T}$ (s) (2)	Flexible-Base $\tilde{\zeta}$ (%) (3)	Fixed-Base T (s) (4)	Fixed-Base ζ (%) (5)	Pseudo-Flexible-Base $\tilde{T}^*$ (s) (6)	Pseudo-Flexible-Base $\tilde{\zeta}^*$ (%) (7)	$\tilde{T}/T$ (s) (8)	$\tilde{\zeta}_0$[a] (%) (9)
Redlands	0.60	4.3	0.59	3.7	0.60	4.2	1.03	0.9
Whittier	0.65	4.4	0.63	5.0	0.64	4.9	1.02	0.0
Upland	0.76	4.7	0.77	7.8	0.78	7.3	1.00	0.0
Landers	0.87	11.2	0.85	12.5	0.86	12.7	1.01	0.0
Northridge	0.76	4.6	0.75	6.9	0.76	6.4	1.02	0.0

[a]Foundation damping factor, computed as $\tilde{\zeta}_0 = \tilde{\zeta} - \zeta/(\tilde{T}/T)^3$

Fig. 2(a) shows first-mode shapes for the Whittier and Landers earthquakes established from CEM analysis results. Significant isolator flexibility is apparent in both earthquakes but is most pronounced during the relatively strong shaking of the Landers event. Time varying first-mode shapes established from RPEM analyses of the Landers event are shown in Fig. 2(b). Results are shown for time t = 13 s when the shaking is weak, t = 20 s when initial shear waves have arrived and displacements are steadily increasing, t = 30 s when the shaking is strong, and t = 60 s after the principal body waves have passed the site. Results for times t = 13, 20, and 30 s indicate increasing relative isolator flexibility as the amplitude of shaking increases. By time t = 60 s, the amplitude of shaking has decayed and the mode shape resembles that for the early portions of the time history before the main shear wave arrivals. These data indicate that the effective first-mode shape is strongly dependent on the amplitude of shaking as a result of nonlinear isolator response.

Inertial soil-structure interaction effects on the structural response are evaluated from first-mode periods and damping ratios established by CEM procedures for the fixed- and flexible-base cases. These modal vibration parameters are shown in Table 3 along with results for the pseudo-flexible-base case and computed period lengthening ratios, $\tilde{T}/T$, and foundation damping factors, $\tilde{\zeta}_0$. This foundation damping factor, introduced by Jennings and Bielak (1973), quantifies the effects of radiation damping and hysteretic soil damping. The overall damping factor of the interacting soil-foundation-structure system, $\tilde{\zeta} = \tilde{\zeta}_0 + \zeta/(\tilde{T}/T)^3$, has components of foundation damping, $\tilde{\zeta}_0$, and structural damping, ζ. In Table 3, the values of period lengthening near unity and essentially zero foundation damping indicate that inertial soil-structure interaction had a negligible influence on the structural response for the FCLJC. Similar results were obtained for the other buildings considered.

Compiled Results for All Sites

RPEM analyses were performed to evaluate the time-varying first-mode frequency and damping ratio for each structure and earthquake listed in Table 1. Figs. 3(a–c) show results for the following examples: LA2FCCB (Sierra Madre earthquake), LA7USC (Northridge earthquake), and SB8 (Landers earthquake). The characteristic behavior of the isolated structure is different in each case, as discussed below.

- As illustrated in Fig. 3(a), the LA2FCCB experienced rapid reduction of the first-mode frequency during the first significant deformation pulse in the isolators, and gradual recovery toward the initial value as the shaking subsequently decayed. During the relatively modest shaking of the Sierra Madre [Fig. 3(a)] and Landers (not shown)

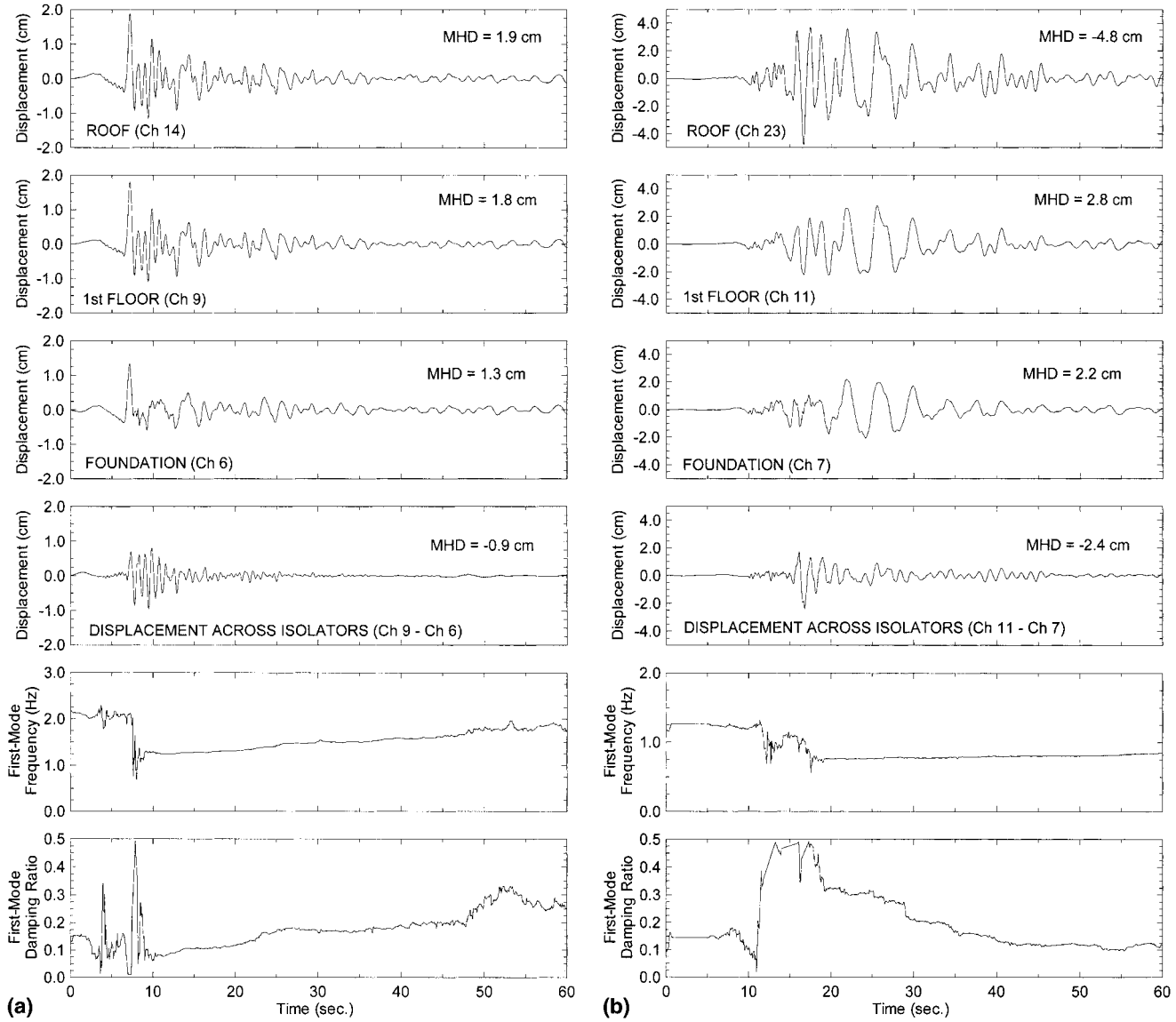

FIG. 3. Displacement Time Histories and Time Variation of First-Mode Parameters: (a) LA2FCCB, 1991 Sierra Madre Earthquake (Transverse, EW Direction); (b) LA7USC, 1994 Northridge Earthquake (Transverse, EW Direction); (c) SB8, 1992 Landers Earthquake (Transverse, NS Direction)

earthquakes, the damping ratio increased gradually as the isolators stiffened during the interval of ground motion decay. An explanation for this trend is provided later. The stronger shaking of the Northridge earthquake (not shown) caused relatively high damping during the main shear wave arrivals, but this damping decayed subsequently.

- During the Northridge earthquake, the LA7USC exhibited sustained frequency reduction and damping increase during the shear wave arrivals from about 11–18 s [Fig. 3(b)]. The identification is somewhat unstable over this time interval, and the damping values shown in Fig. 3(b) during this interval may not be correct. However, the general trends are meaningful, showing a large increase in damping at 11 s and gradual decay after 18 s. Gradual stiffness recovery for $t > 18$ s is also evident. It should be noted that LA7USC is an irregularly shaped building, and hence the response reported here represents a centroidal lateral response as the instruments used for identification are located near the building centroid. A detailed analysis of torsional effects is beyond the scope of this study.
- During the Landers earthquake, the SB8 building exhibited frequency reductions and temporary damping increases during ''pulses'' of isolator deformation that significantly exceed the amplitude of previous pulses [Fig. 3(c)]. These effects are especially apparent during deformation pulses at 33 and 49 s. Modest recovery in the isolation system was observed following the main shear wave arrivals.

The influence of shaking intensity on isolator behavior noted for the FCLJC in the previous section was also observed in the results for LA2FCCB, LA7USC, and SB8. These effects are investigated by compiling two measures of isolator behavior for all earthquakes recorded at each of the four sites. One measure of isolator behavior, termed ''frequency reduction,'' is the maximum reduction in first-mode frequency that occurs in the structure during strong shaking normalized by the initial first-mode frequency for that earthquake. Frequency reduction is evaluated from the results of the RPEM analyses. The second measure of response behavior, termed ''relative isolator deflection'' (RID) is the fraction of total roof displacement (relative to the foundation) contributed by the lateral displacement in the isolators. RID is evaluated using first-mode shapes estimated from CEM analysis. Both measures are compiled in

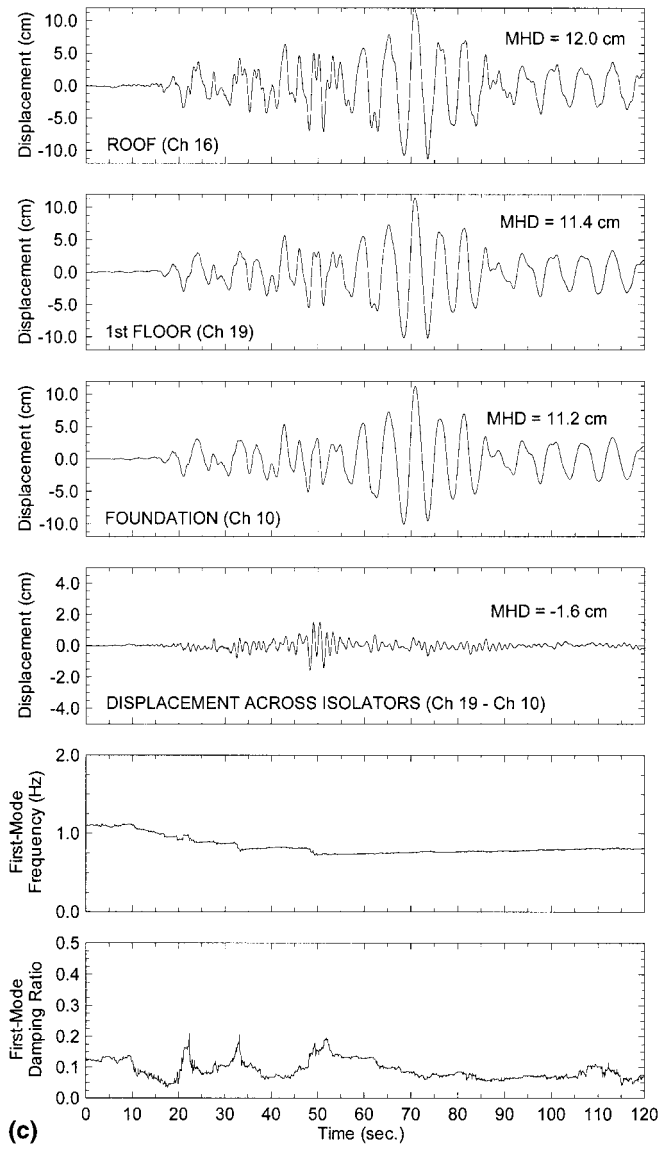

FIG. 3. (*Continued*)

TABLE 4. Frequency Reduction and Relative Isolator Deflection for Subject Sites Computed from CEM System Identification

Site (1)	Earthquake (2)	Frequency reduction (3)	Relative isolator deflection (4)
LA 2-story	Sierra Madre	0.38	0.99
	Landers	0.54	0.94
	Northridge	0.53	1.06
LA 7-story	Landers	0.29	0.28
	Northridge	0.33	0.27
FCLJC	Redlands	0.03	0.10
	Whittier	0.06	0.12
	Upland	0.13	0.21
	Landers	0.23	0.23
	Northridge	0.07	0.18
SB 8-story	Landers	0.35	0.12
	Northridge	0.22	0.02

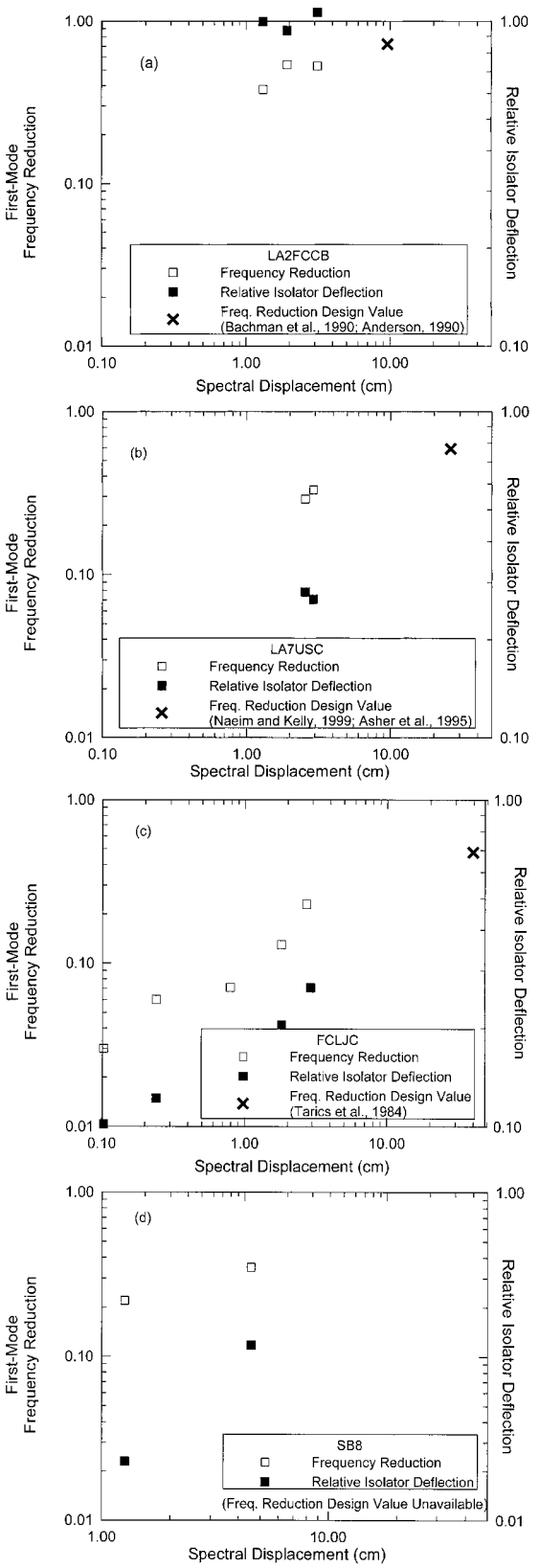

FIG. 4. Variation in Frequency Reduction and Relative Isolator Deflection with Spectral Displacement of Free-Field Motion

Table 4 and plotted in Fig. 4 against the 5% damped free-field spectral displacement at the time-averaged building fundamental period (i.e., from the CEM analyses).

Of the results shown in Fig. 4, only the recordings at the FCLJC and SB8 span a sufficient range of spectral displacement to observe trends. At these two sites, significant increases in frequency reduction and RID with increasing spectral displacement are observed. These results illustrate the strong dependence of isolator flexibility on ground motion amplitudes from different earthquakes. This finding is consistent with intraevent variations of isolated building fundamental-mode frequency and mode shape discussed previously (Figs. 1–3).

Where available, the fundamental-mode vibration frequency used in design is used with average small strain building fre-

quencies from Figs. 1 and 3 to calculate effective ''design values'' of frequency reduction. These design values are plotted in Fig. 4 against the design basis spectral displacement (for the FCLJC), or an estimate of spectral displacement taken as the design basis isolator displacement (for the LA2FCCB and LA7USC). The trend observed in Fig. 4(c) for the FCLJC supports the design value of frequency reduction. For the LA2FCCB and LA7USC buildings, the design values of frequency reduction are consistent with the relatively weak trends apparent from the field performance data. Hence, based on extrapolation of the limited field performance data currently available, it appears that the fundamental-mode vibration frequencies used in the design of the FCLJC, LA2FCCB, and LA7USC are reasonable.

Design data from which to determine RID values were not available, but as noted in the introduction, in the ''ideal'' isolated building, the isolator displacement is much greater than the superstructure displacement. For a truly rigid superstructure, RID = 1.0. This is clearly not the case for the buildings examined, except for LA2FCCB. However, strong increases in RID with spectral displacement are apparent from the data for FCLJC (where a trend can be observed), and values approaching 1.0 at the design spectral displacement of 40 cm appear to be reasonable.

To further investigate variations in isolator behavior during earthquake shaking, an approximation of the nonlinear force-deformation response of the entire isolation system is obtained by plotting the deformation of the isolators against the total acceleration immediately above the isolators, which is proportional to the total shear force imparted to the isolators (assuming a very stiff superstructure). These ''global hysteresis loops'' are presented in Fig. 5 for one earthquake event at each site. The loops are plotted for time increments that begin with small amplitude pressure wave arrivals and continue through the passage of the largest amplitude shear waves. The motions used to develop the plots in Fig. 5 were bandpass filtered to emphasize the frequency content near the first-mode frequency (cutoff frequencies are indicated on the figure). In each case, a stiff initial response is followed by relatively broad hysteresis loops during the strong shear wave arrivals. These results provide direct evidence of the nonlinear hysteretic behavior of the isolator elements, even at low shear strains.

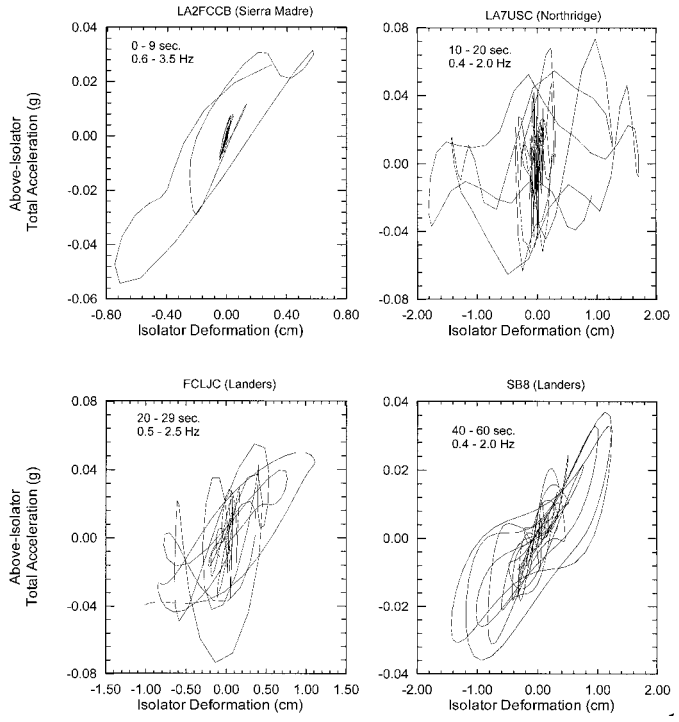

FIG. 5. Approximate Force-Deformation Behavior of Isolation Systems during Selected Earthquakes

INTERPRETATION

Isolator Properties Used in Design, FCLJC

The FCLJC has been designed to withstand, without suffering permanent damage to the basic structure, an estimated maximum credible earthquake (MCE) defined as an $M_w = 8.3$ event on the San Andreas Fault, 22 km from the site. The design basis motion for the MCE had a PGA = 0.6 g, a 5% critically damped design response spectrum with a constant pseudo-velocity of 127 cm/s over the period range [0.8–4.0] s (giving the spectral displacement $S_d = 127/[2\pi(0.50)] = 40$ cm at 2.0 s period), and a duration longer than 35–40 s. The bearings were designed to provide a period of the isolated structure of approximately 2.0 s during the MCE. The maximum displacement in the isolators under the MCE was calculated to be 38 cm. As the effective isolator height is 30.5 cm, this level of displacement corresponds to a maximum shear strain of 38/30.5 cm = 125%). For design purposes, however, the 50% shear strain effective stiffness was used (corresponding to 15 cm of isolator lateral displacement). At this level of strain, the shear modulus of the high damping rubber is about 670 kN/m^2 (Tarics et al. 1984).

Four different high-damping rubber compounds were used in the manufacture of the isolators. Each isolator installed in the FCLJC was tested by the manufacturer at shear strains ranging from about 2–4 to 50–65% (Tarics et at. 1984). The stiffness of elastomers exhibits a property known as ''scragging,'' which is an irreversible reduction in modulus due to deformation that occurs when a rubber specimen is first loaded. The effect is more pronounced in high-damping rubber compounds than in natural rubber formulations. (Another modulus reduction phenomena, known as Mullins' effect, is temporary and recoverable). First cycle (unscragged) and tenth cycle (fully scragged) effective stiffnesses were obtained in the manufacturer's tests, and the resulting effective stiffness for the complete system of 98 bearings are reported in Table 5. Equivalent damping ratio versus shear strain relations for the isolators were evaluated from hysteresis curves derived from force-displacement testing of FCLJC prototype bearings, as well as from tuning-fork/double-shear testing of small rubber coupon specimens. Selected results of these tests are summarized in Table 6.

It may be observed from Tables 5 and 6 that as shear strain increases from a minimum of 2–4 to a maximum of 50–65%, the effective stiffness and damping decrease. While this trend of stiffness reduction with increasing shear strain is consistent with the fundamental-mode frequency results in Fig. 1, the damping trends from the field and laboratory data appear to

TABLE 5. Effective Shear Stiffness for Complete Isolation System (after Tarics et al. 1984)

Isolation system property (1)	Shear Strain 2% (2)	10% (3)	25% (4)	50% (5)
Unscragged stiffness[a] (Isolation period)[b]	8,661 (0.79 s)[a]	4,004 (1.16 s)	2,471 (1.47 s)	1,671 (1.79 s)
Scragged stiffness[a] (Isolation period)[b]	2,975 (1.34 s)	1,750 (1.75 s)	1,400 (1.96 s)	1,120 (2.18 s)

[a]Effective stiffness in kN/cm, unscragged = 1st cycle, scragged = 10th cycle.

[b]Isolation period = fundamental period assuming the superstructure to be rigid.

TABLE 6. Effective Damping Ratio for Complete Isolation System (after Tarics et al. 1984)

Isolation system property (1)	Shear Strain 3.6% (2)	12% (3)	22% (4)	43% (5)	65% (6)
Unscragged damping[a]	23.3%	20.7%	18.1%	14.6%	13%
Scragged damping[a]	16.5%	14.7%	13.4%	12%	11%

[a]Unscragged = 1st cycle, scragged = 10th cycle.

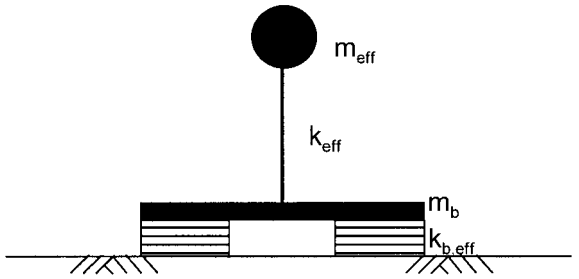

FIG. 6. Two-Degree-of-Freedom Idealization of Seismically Isolated Building

be inconsistent. The following sections provide a more detailed examination of these results.

Comparison of Observed Isolator Stiffness with Laboratory Test Results, FCLJC

For each of the five selected earthquakes, the effective stiffness of the entire isolation system, $k_{b,\text{eff}}$, was inferred based on a simple linear elastic two-degree-of-freedom idealization of the isolated building shown in Fig. 6. Table 1 lists fundamental mode periods of various substructures in Fig. 6, namely, the ''whole building'' period, which corresponds to the period of the isolated building, and the ''above isolators'' period, which corresponds to the period of the portion of the building supported by the isolators. The overall mass of the FCLJC building is 13,200 tons, which is distributed as follows: (1) basement—3,200 tons; (2) 1st floor—3,100 tons; (3) 2nd floor—1,800 tons; (4) 3rd floor—1,800 tons; (5) 4th floor—1,900 tons; and (6) roof—1,400 tons (Tarics et al. 1984; Maison and Ventura 1992).

Based on the model in Fig. 6, the isolated building was decomposed into a rigid substructure of mass m_b equal to the combined basement and first floor masses (6,300 tons), and the superstructure idealized as an SDOF system of effective stiffness k_{eff} and effective mass m_{eff}. The effective mass m_{eff} is defined as the first-mode participating mass (Chopra 1995; Wilson 1998) of the superstructure, assumed to be on the order of 75–90% of the total mass (a range encompassing typical first-mode participating mass ratios for steel moment resisting frames). Superstructure stiffness, k_{eff}, is then computed using m_{eff} and the above-isolator fixed-base fundamental frequency from Table 1. With these values of m_b, m_{eff}, and k_{eff}, the effective stiffness of the complete isolation system, $k_{b,\text{eff}}$, was then inferred by matching the fundamental mode frequency of the two-degree-of-freedom model in Fig. 6 to the CEM whole structure frequency in Table 1. These evaluations of $k_{b,\text{eff}}$ were performed two ways, first assuming a rigid above-isolator superstructure (i.e., $k_{\text{eff}} \rightarrow \infty$), and second accounting for the actual flexibility of the superstructure. Both cases are shown in Table 7 for superstructure participating mass ratios of 75 and 90%. Table 7 also reports the peak and root-mean-square values of the shear strain in the isolators (in the N-S direction) for each earthquake event, computed from the measured displacement differential across the isolators and the known effective isolator height of 30.5 cm. The root-mean-square shear strains were computed over the time interval of 5–95% normalized Arias duration (i.e., the time interval containing roughly the middle-90 percent of earthquake energy).

The inferred effective stiffnesses are significantly larger than the unscragged experimental effective stiffness at 2% shear strain, reported in Table 5. As the root-mean-square shear strains in the isolators for each event were less than 2%, these stiffness variations suggest that the rubber comprising the isolators is characterized by significant stiffness reduction with increasing shear strain for strains less than 2%. At larger shear strains, the experimental results summarized in Table 5 show a similar trend of significant shear stiffness reduction with increasing shear strain. Hence, while the inferred effective stiffnesses of the global isolation system cannot be compared directly with experimental results, due to the lack of available test results at small strains, the field performance data nonetheless reveal that the experimentally determined 2%-strain unscragged stiffness values do not represent the isolator behavior at significantly lower strain levels (~0.1%). In fact, the special rubber compound comprising the isolators exhibits highly nonlinear behavior at shear strains <2%.

Also noteworthy in Table 7 is the importance of accounting for the flexibility of the superstructure (as opposed to assuming a rigid superstructure) in back-calculations of $k_{b,\text{eff}}$ from field performance data involving small isolator strains. The assumption of a rigid superstructure, which has been made in several prior studies, leads to significant overestimates of $k_{b,\text{eff}}$.

Damping in Isolators

In the FCLJC isolator testing program, damping was inferred from results of harmonic shear tests performed on full-scale bearings or small rubber coupons (tuning fork specimens). For the bearing tests, an equivalent damping ratio, ξ_{eq},

TABLE 7. Inferred Effective Stiffness of Complete Isolation System (Assuming First-Mode Participating Mass Ratio of 75 and 90%)

Earthquake (% first-mode participating mass) (1)	Peak and RMS shear strain (%) (2)	K_{eff} (kN/cm) (3)	Inferred Effective Shear Stiffness, $K_{b,\text{eff}}$ (kN/cm) Assuming rigid superstructure (4)	Assuming flexible superstructure (5)
Redlands 75%	0.15%; 0.06%	8,255	15,144	28,000
90%		9,905	15,145	32,200
Whittier 75%	0.42%; 0.12%	7,368	13,060	22,750
90%		8,841	13,060	26,250
Upland 75%	1.43%; 0.66%	4,340	8,703	19,863
90%		5,215	8,703	22,925
Landers 75%	4.39%; 1.40%	5,317	7,147	9,275
90%		6,381	7,147	10,465
Northridge 75%	0.80%; 0.30%	5,355	9,345	15,925
90%		6,423	9,345	18,200

was evaluated for a given shear strain and vertical load level as (Chopra 1995)

$$\xi_{eq} = \frac{1}{4\pi}\frac{1}{\omega/\omega_n}\frac{E_D}{E_{So}} \quad (1)$$

where E_D = energy dissipated per cycle (= area enclosed by hysteresis loop); E_{So} = maximum strain energy stored in a linear elastic system with a stiffness equal to the secant stiffness of the hysteresis loop; ω = forcing circular frequency; and ω_n = (fundamental) natural circular frequency of the system. The harmonic tests were performed at the design target natural frequency of the isolated building of 0.5 Hz. The equivalent (composite) damping ratio for the complete assemblage of 98 bearings was then taken, according to a stiffness-weighted composite model damping technique, as the sum of stiffness-proportional damping ratios of the individual bearings (Tarics et al. 1984).

As noted previously in the observation of Fig. 3, the first-mode damping ratios obtained through recursive modal identification strongly correlate to the shear strain amplitude in the isolator (which is proportional to the displacement across the isolators). This suggests that the damping characteristics of isolation systems at low shear strain levels (below 1%) follow a simple frequency- or rate-independent linear damping model (Chopra 1995), also called a Kelvin-Voigt model, in which the damping force (f_D) takes the form $f_D(t) = (\eta k/\omega)\dot{u}(t)$, where η = a hysteretic damping coefficient, k = stiffness coefficient, ω denotes circular frequency, and $\dot{u}(t)$ = relative velocity response. By equating the viscous energy dissipated per cycle of harmonic straining from the Kelvin-Voigt model to the energy dissipation for a frequency-dependent, linear, viscous damping model [$f_D(t) = c_{eq}\dot{u}(t)$], the equivalent damping coefficient (c_{eq}) and corresponding damping ratio (ξ_{eq}) can be evaluated as $c_{eq} = \eta k/\omega$ and $\xi_{eq} = (\eta/2)(\omega_n/\omega)$. If the equality between the viscous energy dissipated per cycle given by the two models is enforced at $\omega = \omega_n$, which is usually done, then the above relations become $c_{eq} = \eta k/\omega_n$ and $\xi_{eq} = \eta/2$.

The dependence of ξ_{eq} on shaking amplitude [e.g., Figs. 1(b) and 3(a–c)] indicates that at very small shear strains (<1%), the equivalent damping ratio of isolation systems *increases* with shear-strain amplitude, a characteristic long known to exist in soil materials (Seed and Idriss 1970). In contrast, the trend obtained from experimental testing of the FCLJC full-size rubber bearings and small rubber coupons (Tarics et al. 1984) revealed a *decrease* in damping ratio with increasing shear-strain amplitude (see Table 6). Since all the experimental results were obtained at levels of shear strain greater than those experienced by the isolators during the earthquake events studied, there appears to be a transition shear-strain amplitude at which the trend of the damping ratio versus shear strain amplitude reverses. Only experimental testing on full-size rubber bearings and small samples of rubber could confirm the indirect findings of this study and elucidate the actual energy dissipation characteristics of laminated rubber bearings at very small strains (below 1%).

An interesting feature, observed in Fig. 3(a) for example, and in other cases that are not reported here, is an increase in the identified equivalent damping ratio toward the end of the ground motion. This can be explained as follows. Towards the end of an earthquake ground motion, ω_n increases and η decreases due to a decrease in the shear-strain demand, while simultaneously the predominant forcing frequency of the earthquake ω decreases. As the equivalent damping ratio varies as $\xi_{eq} = (\eta/2)(\omega_n/\omega)$ (as given above), the net effect of these changes can be an increase of ξ_{eq} if the increase in ω_n/ω exceeds the decrease in η. This appears to be the case in Fig. 3(a)(LA2FCCB, Sierra Madre earthquake), where the time scale allows the motions (and ξ_{eq}) to be plotted to times significantly beyond the relatively short interval of body wave passage. In contrast, time histories for larger magnitude earthquakes [e.g., Landers and Northridge earthquakes, Figs. 1(b), 3(b–c)] do not extend sufficiently long following body wave passage, meaning that long-period, low amplitude site oscillations and surface waves do not dominate the motions at the end of the plotted time history to the same extent as in the Sierra Madre earthquake [Fig. 3(a)]. This may explain the lack of any pronounced damping increase late in the time histories for these cases.

CONCLUSIONS

The response of four base-isolated buildings during six recent California earthquakes was investigated in this study. All four buildings were found to have experienced frequency reduction during earthquake shaking that correlated well with large amplitude pulses of ground motion. The observed frequency reduction (or period lengthening) was not nearly as large as assumed for the design basis earthquakes. Three of the four buildings were found to have experienced significant amplification of ground motion above the isolators over the height of the structure, which contrasts with the common design assumption of negligible superstructure amplification. Another common design assumption, that soil-structure interaction effects are negligible, was found to be reasonable for the subject seismically isolated buildings.

Two measures of isolation system behavior, the maximum reduction of the effective fundamental mode frequency during strong shaking and the percentage of total building deformation occurring within the isolators, were found to correlate well with the spectral displacement at the effective period of the isolated building. Extrapolations of the observed trends for frequency reduction to larger (design) levels of spectral displacement are consistent with the level of performance assumed in design.

The stiffness and damping of the seismic isolation systems were isolated and evaluated. The systems were found to respond with a hysteretic action that is strongly dependent on shaking amplitude. In the case of the FCLJC building, inferred effective stiffnesses of the isolation system are significantly higher than the experimentally determined unscragged stiffness at 2% shear strain. In each case the root-mean-square isolator shear strain over the duration of strong shaking was well below 2% (the minimum shear strain at which the bearings were tested). Hence this field performance data indicates that, at small strain levels, the isolators are much stiffer than suggested by experiments conducted at 2% strain, and that the isolators are subject to significant stiffness reduction with increasing shear-strain amplitude.

Damping values obtained from system identification analyses suggest that at small shear-strain amplitudes (<1%), damping characteristics of the isolation systems follow the frequency-independent, linear Kelvin-Voigt damping model widely used to model hysteretic damping in soil materials. Thus the identification results suggest that, at low strains, the equivalent viscous damping ratio of the isolation system increases with the level of shear strain (as in the case of soil materials), which is opposite the trend of decreasing damping ratio versus shear strain obtained experimentally above 2% shear strain for the FCLJC bearings.

The differences between the isolation system stiffnesses (and fundamental periods) derived from system identification of measured earthquake response and the original design values (e.g., for LA2FCCB, LA7USC, and FCLJC) highlight the importance of carefully considering the ground motion amplitude when investigating and assessing the behavior of isolated structures in small to moderate earthquakes. For such events,

fully softened isolator stiffness and damping values from laboratory tests do not appear to provide an accurate measure of actual isolator behavior. Moreover, significant amplification of ground motion over the height of the superstructure may occur under these conditions. These considerations may be significant for the design of nonstructural elements or sensitive equipment in seismically isolated buildings.

ACKNOWLEDGMENTS

Support for this project was provided by a CAREER grant from the National Science Foundation through the Earthquake Hazards Reduction Program (NSF Award No. CMS-9733113). This support is gratefully acknowledged. The views and conclusions contained in this document are those of the writers and should not be interpreted as necessarily representing the official policies, either expressed or implied, of the U.S. Government. We would also like to thank the anonymous reviewers of this document for their helpful comments.

APPENDIX. REFERENCES

Anderson, T. L. (1990). ''Seismic isolation design and construction practice.'' *Proc., 4th U.S. Nat. Conf. on Earthquake Engrg.*, Earthquake Engineering Research Institute, El Cerrito, Calif., 519–528.

Asher, J. W., Hoskere, S. N., Ewing, R. D., Van Volkinburg, D. R., Mayes, R. L., and Button, M. R. (1995). ''Seismic performance of the base isolated USC University Hospital in the 1994 Northridge earthquake.'' *Seminar on Isolation, Energy Dissipation and Control of Vibration of Struct.*, ASME, New York, August 21–23.

Bachman, R. E., Gomez, M. J., and Chang, K. C. (1990). ''Verification analysis of the base isolated Los Angeles Fire Command and Control Facility.'' *Proc., 4th U.S. Nat. Conf. on Earthquake Engrg.*, Earthquake Engineering Research Institute, El Cerrito, Calif., 539–548.

Chopra, A. K. (1995). *Dynamics of structures—theory and applications to earthquake engineering*, Prentice-Hall, Englewood Cliffs, N.J.

Jennings, P. C., and Bielak, J. (1973). ''Dynamics of building-soil interaction.'' *Bull. Seismology Soc. Am.*, 63, 9–48.

Kelly, J. M., Aiken, I. D., and Clark, P. W. (1991). ''Response of base-isolated structures in recent California earthquakes.'' *Proc., SMIP91 Seminar on Seismolog. and Engrg. Implications of Recent Strong-Motion Data*, California Strong Motion Instrumentation Program, Sacramento, Calif.

Maison, B. F., and Ventura, C. E. (1992). ''Seismic analysis of base-isolated San Bernardino County building,'' *Earthquake Spectra*, 8(4), 605–633.

Makris, N., and Deoskar, H. S. (1996). ''Prediction of observed response of base-isolated structure.'' *J. Struct. Engrg.*, ASCE, 122(5), 485–493.

Naeim, F., and Kelly, J. M. (1999). *Design of seismic isolated structures: From theory to practice*. Wiley, New York.

Nagarajaiah, S., and Xiahong, S. (1995). ''Response of base isolated buildings during the 1994 Northridge earthquake,'' *Proc., SMIP95 Seminar on Seismolog. and Engrg. Implications of Recent Strong-Motion Data*, California Strong Motion Instrumentation Program, Sacramento, Calif.

Papageorgiou, A. S., and Lin, B.-C. (1989). ''Study of the earthquake response of the base-isolated law and justice center in Rancho Cucamonga.'' *Earthquake Engrg. and Struct. Dyn.*, 18, 1189–1200.

Pardoen, G. C., and Hart, G. C. (1985). ''Modal analysis of a base isolated building.'' *Proc., 3rd Int. Modal Anal. Conf.*, Union College, Schenectady, N.Y., 1312–1316.

Safak, E. (1989a). ''Adaptive modeling, identification, and control of dynamic structural systems. I: Theory.'' *J. Engrg. Mech.*, ASCE, 115(11), 2386–2405.

Safak, E. (1989b). ''Adaptive modeling, identification, and control of dynamic structural systems. II: Applications.'' *J. Engrg. Mech.*, ASCE, 115(11), 2406–2426.

Safak, E. (1991). ''Identification of linear structures using discrete-time filters.'' *J. Struct. Engrg.*, ASCE, 117(10), 3064–3085.

Seed, H. B., and Idriss, I, M. (1970). ''Soil moduli and damping factors for dynamic response analyses.'' *Rep. No. EERC 70-10*, Earthquake Engineering Research Ctr., University of California, Berkeley, Calif.

Stewart, J. P., and Fenves, G. L. (1998). ''System identification for evaluating soil-structure interaction effects in buildings from strong motion recordings.'' *Earthquake Engrg. and Struct. Dyn.*, 27, 869–885.

Stewart, J. P., Fenves, G. L., and Seed, R. B. (1999). ''Seismic soil-structure interaction in buildings. II: Empirical findings.'' *J. Geotech. and Geoenvir. Engrg.*, ASCE, 125(1), 38–48.

Stewart, J. P., and Stewart, A. F. (1997). ''Analysis of soil-structure interaction effects on building response from earthquake strong motion recordings at 58 sites.'' *Rep. No. UCB/EERC-97/01*, Earthquake Engineering Research Ctr., University of California, Berkeley, Calif.

Tarics, A. G., Way, D., and Kelly, J. M. (1984). ''The implementation of base isolation for the Foothill Communities Law and Justice Center.'' *A Report to the National Science Foundation and the County of San Bernardino*, Reid and Tarics Associates, San Francisco, Calif.

Wilson, E. L. (1998). *Three Dimensional Static and Dynamic Analysis of Structures*. Computers and Structures, Inc., Berkeley, Calif.